Longitudinal variation of the E-region electric fields caused by atmospheric tides

S. L. England,[1] S. Maus,[2] T. J. Immel,[1] and S. B. Mende[1]

Received 5 July 2006; revised 21 September 2006; accepted 4 October 2006; published 4 November 2006.

[1] Polarization electric fields created by the E- and F-region dynamos cause the uplift of F-region plasma. The subsequent redistribution of that plasma along the magnetic field lines creates the equatorial ionospheric anomaly (EIA). Observations of the post-sunset EIA made by the IMAGE and TIMED satellites are compared here with CHAMP, Ørsted and SAC-C observations of the noontime equatorial electrojet (EEJ). During magnetically quiet periods around equinox, the EIA and EEJ show a remarkably similar four-peaked wave-like longitudinal variation. Its structure is consistent with the longitudinal variation in the strength of diurnal tides that drive the E-region dynamo. This indicates a strong vertical coupling between the ionosphere and troposphere because the four-peaked tidal structure is driven by tropospheric weather. Furthermore, the dayside ionospheric conditions are found to perform the global-scale longitudinal structure of the post-sunset ionosphere at low latitudes. **Citation:** England, S. L., S. Maus, T. J. Immel, and S. B. Mende (2006), Longitudinal variation of the E-region electric fields caused by atmospheric tides, *Geophys. Res. Lett.*, *33*, L21105, doi:10.1029/2006GL027465.

1. Introduction

[2] While the highest ion production rates in the ionosphere are found at the sub-solar point, the peak ion densities are located several degrees to either side of the magnetic equator. This feature, the equatorial ionospheric anomaly (EIA), is created by a fountain effect, that involves the uplift of plasma at the magnetic equator by eastward polarization electric fields and redistribution of that plasma along the magnetic field lines which map to higher latitudes. During solar quiet periods, these polarization fields are created by a combination of Pedersen current driven by poleward winds in the E-region [*Tarpley*, 1970] and the F-region dynamo [*Rishbeth*, 1971]. While the E-region dynamo dominates vertical drifts at most local times, the F-region dynamo is responsible for the strong vertical drift of plasma around sunset [*Farley et al.*, 1986].

[3] Recent observations using the IMAGE and TIMED satellites have revealed a global wavenumber-four longitudinal signature in the equatorial nighttime airglow intensities and position of the EIA and associated airglow arcs in the F-region ionosphere around equinox [*Henderson et al.*, 2005a; *Sagawa et al.*, 2005]. *Immel et al.* [2006] have demonstrated that this could be explained by a longitudinal variation in the diurnal amplitude of atmospheric tides in the E-region ionosphere. An increase in the observed separation of the airglow arcs and a coincident strong increase in the peak ion density in the arcs is indicative of an effect that takes place while ion production is still occurring, such as a modulation of the dayside fountain in response to a variation in the tidal winds in the E-region. However, from post-sunset observations alone, it is not possible to directly confirm that the wavenumber-four signature is not the result a modification of the strong vertical drifts around sunset associated with the F-region dynamo. This is usually considered to be the dominant factor in determining conditions of the post-sunset equatorial ionosphere, especially close to solar maximum. Modulation of the E-region tidal amplitudes will produce a change in the Pedersen currents and associated eastward polarization electric fields that are responsible for the E-region dynamo. Detecting such a zonal wavenumber-four structure in the electric currents driven by the E-region dynamo would confirm that the E-region electric fields and associated fountain is likely responsible for the variation of the EIA, as observed in the early evening by the IMAGE and TIMED satellites.

[4] The equatorial electrojet (EEJ) is a narrow band of intense electric current that flows in the dayside E-region, following the magnetic equator at approximately 108 km altitude. The EEJ is driven by the eastward electric field in the equatorial E-region ionosphere that also drives the equatorial fountain. Early space-based observations of the EEJ offered the ability to characterize the longitudinal variability of its parameters. However, studies using the OGO satellites [e.g., *Onwumechili and Agu*, 1981; *Kim and King*, 1999] and Magsat [e.g., *Ravat and Hinze*, 1993] appeared to produce somewhat contradictory results, which is perhaps not surprising given the very limited amount of data available and the extremely large variability in satellite observations of the EEJ [cf. *Lühr et al.*, 2004] and discrepancies in the local time (LT) and season of different measurements. Recent low altitude satellite observations of magnetic field data have allowed the spatial structure of this current system to be measured to with high resolution over all longitudes [*Jadhav et al.*, 2002; *Ivers et al.*, 2003; *Lühr et al.*, 2004; *Doumouya and Cohen*, 2004; *Manoj et al.*, 2006]. These therefore offer the ideal dayside complement to the nightside IMAGE and TIMED observations described above. Observations of the EEJ also have the advantage of being less affected by other external forces such as winds at F-region altitudes.

[5] Here we shall use observations of the EEJ from the SAC-C, Ørsted and CHAMP satellites over a total of five years to characterize the longitudinal structure of the EEJ and compare this to the IMAGE and TIMED observations

[1] Space Sciences Laboratory, University of California Berkeley, Berkeley, California, USA.
[2] Cooperative Institute for Research in Environmental Sciences, University of Colorado, Boulder, Colorado, USA.

0094-8276/06/2006GL027465$05.00

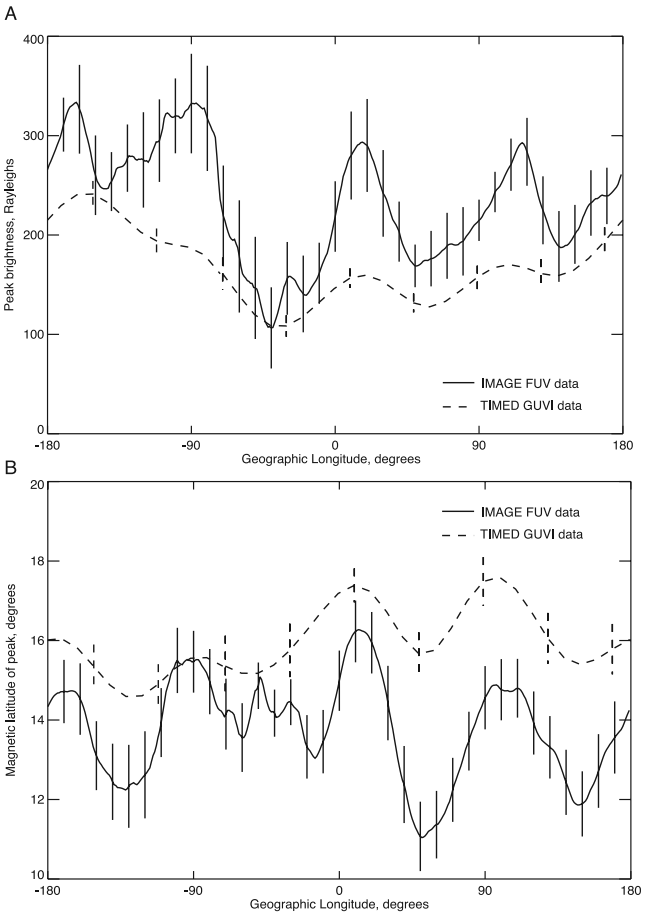

Figure 1. (a) Magnetic latitude of the peak 135.6 nm emission rates and (b) brightness of this peak observed in the northern arc of the EIA by IMAGE FUV (solid) and TIMED GUVI (dashed). Values have been averaged with a 10-degree running mean and assume a mean emission altitude of 350 km. All data come from 20:30 to 21:30 LT, during magnetically quiet periods from March and April 2002. Errors are estimated from the spread of the data and uncertainties in mapping.

of the EIA. Section 2 shall describe the satellite data used, with particular emphasis on the EEJ data which has not previously been published in the form presented here. Section 3 will discuss the comparison of the EIA and EEJ data to one another and to results from the Global Scale Wave Model 2002 (GSWM) [*Hagan and Forbes*, 2002]. We shall demonstrate a clear correspondence between these two types of observations and further establish that longitudinal structure of the EEJ and EIA during magnetically quiet equinoctial periods is dominated by the structure in the propagating diurnal tides in the dayside equatorial lower thermosphere and ionosphere.

2. Data Selection and Analysis

2.1. Far Ultra-violet Observations of the EIA

[6] The far ultra-violet (FUV) observations of the EIA by the IMAGE FUV and TIMED GUVI instruments that will be considered here have been recently presented by *Immel et al.* [2006]. Our analysis of these data is identical to that performed by these authors, so only the key points will be iterated here. Our analysis is restricted to equinoctial periods and the only extended period for which the EIA could be characterized by both IMAGE and TIMED was during March–April 2002. In order to avoid the effects of electric fields of magnetospheric origin, only magnetically quiet periods (the mean K_p over the previous 0–6, 7–12, 12–18 and 18–30 hours was less than or equal to three) were included. To avoid the nighttime eastward drifts from smearing the observed longitudinal structure of the EIA, data from only one hour of local time are used. 20:30–21:30 LT is selected as this is close to sunset and hence the FUV emissions are still bright and avoids overlap with the effects of the pre-reversal enhancement. Fitting routines outlined by *Henderson et al.* [2005b] and *Immel et al.* [2006] were used to define the peak value and location of the 135.6 nm F-region O^+ recombination emissions. These values and locations are plotted as a function of longitude at this fixed local time in Figure 1.

2.2. Magnetic Field Observations of the EEJ

[7] The simultaneous availability of high quality magnetic field measurements from three polar, low-orbiting satellites, CHAMP, Ørsted and SAC-C, provides unprecedented information on the longitudinal structure of the EEJ and associated dayside E-region electric fields. Each satellite passes the day-side equatorial region in the meridional direction once every 90 minutes. The EEJ is most easily observed close to local noon, when the E-region conductivity peaks. For this reason, only data from 10:00–14:00 LT are included in this study. In a similar manner to the FUV data, total-intensity magnetic measurements are selected for magnetically quiet periods ($K_p \leq 2$), for 45 days before and after vernal and autumnal equinox. Details of the satellites and selected data are summarized in Table 1.

[8] The EEJ current densities are estimated by an improved version of the method used by *Lühr et al.* [2004]. From the magnetic measurements of each satellite pass, we subtract the POMME-3.1 model [*Maus et al.*,

Table 1. Summary of Magnetic Satellite Data Used in This Study[a]

	CHAMP	Ørsted	SAC-C
Time period used	2000.6–2003.5	1999.5–2003.5	2001.0–2003.3
Local time coverage used	10–14	10–14	10:30
Passes satisfying selection criteria	1146	1159	2684
Spacecraft altitude (km)	350–450	650–850	700
Spacecraft inclination	87.3°	96.5°	98.2°
Local time drift of spacecraft	−1h in 11 days	−1h in 64 days	Constant

[a]While CHAMP and Ørsted provide data across the 10–14 LT interval, SAC-C remains at 10:30 LT and hence provides the largest number of data points within our window, despite the instrument's relatively short operational lifetime.

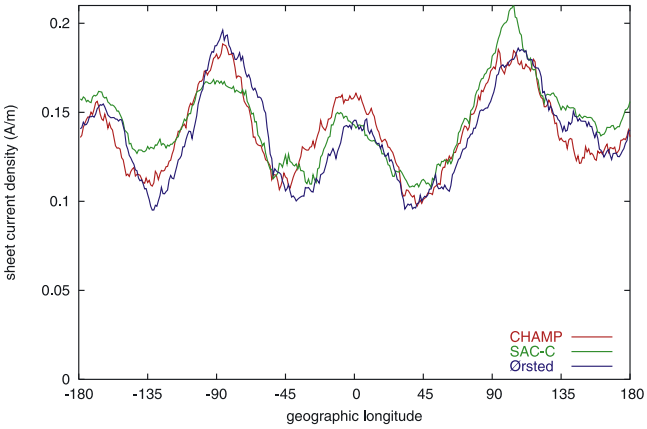

Figure 2. Peak of the noontime electrojet sheet current density as a function of longitude for geomagnetically quiet periods ($K_p \leq 2$) around the March equinox derived from CHAMP, SAC-C and Ørsted magnetic field measurements. The local time and date ranges for each instrument are summarized in Table 1.

2006] to remove contributions from the core, mantle, crust, and magnetosphere. We then find the background Sq signal by fitting a spherical harmonic degree-12 function to the magnetic residuals in the ±60° magnetic latitude range, sparing a ±8° window about the dip equator, which contains the magnetic signal of the EEJ. After subtracting this background field estimate, the residual magnetic signal is inverted for line currents, spaced 0.5 degrees apart, following constant quasi-dipole latitudes at 108 km altitude. Each satellite pass thus yields a profile of line currents. Since the zero level of the current is not well constrained, we use as the relevant parameter the difference between the current at the (exact) dip equator and the average of the northern and southern current troughs. Physically, this is the difference between the equatorial eastward and (possible) adjacent westward return currents. The data set of one current difference per satellite pass is then smoothed by a running mean, using a window of 20° in longitude. Figure 2 shows the longitudinal structure in the noontime EEJ thus inferred from each of the three satellites. While we have not estimated the errors associated with each individual profile, the excellent agreement between the three different data sets gives us a measure of the uncertainty in our retrieval of this longitudinal structure. Further, given the very different sampling of the three spacecraft in universal time, the agreement between the three results also demonstrates that the longitudinal structure of the EEJ is relatively steady throughout the sampling window and across multiple years.

3. Discussion

[9] From Figure 1 it can be seen that perturbations in the brightness of the airglow arcs of a factor of ~2–3 are seen as a function of longitude, which correspond to changes in the nighttime F-region O^+ density of $\sim\sqrt{2}-\sqrt{3}$. Modulation of the mean of the peak sheet current density of the EEJ of a factor of two are seen in Figure 2. Comparing Figures 1 and 2, it is clear that there is a striking correlation between the longitudinal structure of the post-sunset EIA and noon-time EEJ during magnetically quiet periods around equinox. This provides strong evidence that the two processes are correlated, at least in the long-term mean and at large-scales. It should be stressed here that the wavenumber-four signatures shown in Figures 1 and 2 are not statistical structures that only emerge in the long-term mean for a large number of observations. In fact, this structure is consistently visible, even in a single day of FUV or EEJ observations.

[10] The 135.6 nm emissions used by IMAGE and TIMED to measure the EIA are highly sensitive to solar UV flux as the emission brightness depends upon the product of the electron and ion density in the ionosphere. This, combined with the precession of the IMAGE orbit giving unfavorable viewing geometry in 2000–2001, means that only data from 2002 is used to characterize the EIA in this study. However, the magnetic field data can be used to detect the EEJ over several years. Having established the connection between the longitudinal behavior of these two systems, we may now say that the process which creates the four-peaked longitudinal structure in the quiet-time equinoctial EIA is likely present during years away from solar maximum, which could not be confirmed from the FUV data alone. It should be noted however that as the EIA and associated airglow arcs are influenced by meridional winds in the F-region [*Thuillier et al.*, 2002], a simple wavenumber-four pattern may not necessarily be the dominant pattern during all magnetically quiet periods around equinox.

[11] Both the brightness and latitude of the nighttime FUV emissions can be modified by a number of processes. *Sagawa et al.* [2005] found that the wavenumber-four structure observed by IMAGE FUV could not be explained by magnetic declination, magnetic field strength or the offset between magnetic and geographic equators. Further to the discussion presented by the *Sagawa et al.* [2005], while F-region meridional winds can affect the FUV emissions, we are aware of no known theory, model or observation which would support the existence of a wavenumber-four structure in the F-region meridional winds that would be required to reproduce the structure shown in Figure 1. Vertical drifts in the F-region ionosphere can create both changes in the brightness and latitude of the FUV emissions. As can be seen from the nighttime evolution of the FUV emissions presented by *Sagawa et al.* [2005], the nighttime vertical drifts associated with the E-region dynamo are unable to account for the changes in the FUV brightness at 21:00 LT shown in Figure 1 as the combined effects of these drifts and loss due to O^+ nighttime recombination on the FUV brightness is too slow by at least a factor of 3–4. This leaves only the daytime vertical drifts associated with the E-region dynamo and the strong vertical drifts associated with the F-region dynamo as plausible sources of the wavenumber-four pattern shown in Figure 1. An increase in the strength of the E-region dynamo and associated dayside fountain at any specific location leads to an increase the latitude of the F-region plasma distribution. An increase in the strength of the dayside fountain also leads to enhanced F-region ion production, as the system is driven further away from photochemical equilibrium, resulting in an increase in the F-region plasma density and FUV emissions. A change in the strength of the vertical drifts around sunset associated with the F-region dynamo may also affect the

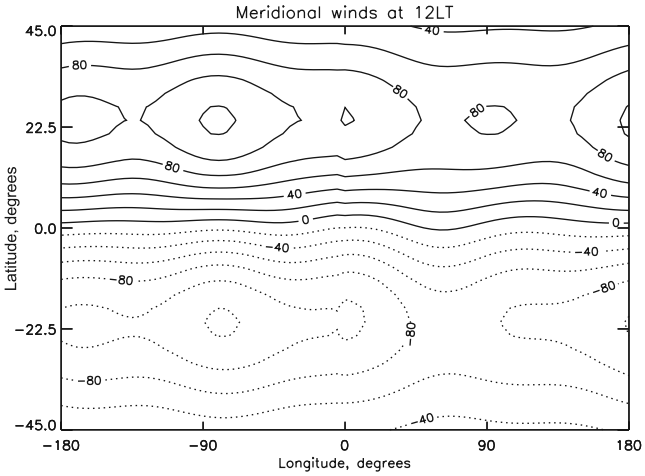

Figure 3. Meridional winds at 12 LT and 107 km altitude associated with the combined diurnal tidal components calculated by the GSWM-02 model for April conditions. Positive denotes northward winds. Southward winds are shown by the dashed line.

latitude and brightness of the FUV emission. The strength of this effect on the FUV emissions is difficult to quantify as these drifts occur too close to sunset for the nighttime FUV observations to be entirely reliable. The F-region dynamo does not impact upon the strength of the EEJ and, as stated above, there is no reason to believe that a modulation of either the F-region winds or the conductivity profiles which determine its strength would have a wavenumber-four signature (except possibly via preconditioning involving the E-region dynamo [*England et al.*, 2006]). Further, given the striking similarity of the wavenumber-four signatures observed in the EEJ and EIA, it seems highly unlikely that these two signatures are created by unrelated processes, and therefore the ultimate source of the observed signatures cannot be a modulation of the F-region dynamo. Thus, by considering both the EIA and EEJ observations together, we can say that while all of the above effects doubtlessly contribute in some way to the observed structure of the nighttime EIA, the source of the wavenumber-four signature in the EIA and EEJ is a modulation of the E-region dynamo fields and associated vertical drifts in the F-region ionosphere.

[12] The E-region dynamo is driven by poleward neutral winds in the thermosphere at E-region altitudes [see *Heelis*, 2004 and references therein]. Any process that can modulate either these winds or the electric fields that they create can modify the strength of the equatorial fountain. *Immel et al.* [2006] demonstrated that the longitudinal perturbation in the tidal winds in the E-region ionosphere could be responsible for the modulation of the EIA via a modulation of the E-region dynamo. Figure 3 shows the 12 LT meridional winds associated with the combined diurnal tidal components calculated by the GSWM for April conditions at 107 km altitude (data from *Hagan and Forbes* [2002]), which is close to where the tidal amplitude peaks and the EEJ currents are found. Around equinox, the meridional winds associated with these waves dominate the wind structure at this altitude. The clear wavenumber-four pattern in the low-latitude winds is primarily the result of an eastward propagating wavenumber-three non-migrating diurnal tide which is being viewed in the westward rotating constant LT reference frame. This wind pattern peaks around 12 LT and as these waves have a 24-hour periodicity, the reverse pattern is present at 00 LT (the winds flow towards the equator), with minima in the wind strength around 6 and 18 LT. The 180° longitude symmetry of the amplitude of the wind modulations means that interactions between these winds and the E-region ionosphere during both day and night produce electric fields which reinforce one another and vary in strength in the same manner as local noon moves in longitude. As discussed by *Immel et al.* [2006], these tidal changes in the strength of the winds are responsible for creating a longitudinal modulation of the E-region dynamo fields and associated daytime upward drift of F-region plasma. Here we see evidence that this longitudinal/local time modulation of the E-region dynamo affects not only the post-sunset F-region plasma distribution, but also the noontime EEJ. The joint analysis of EEJ magnetic signatures and FUV observations of the EIA therefore offers intriguing opportunities for further studies of the equatorial ionosphere.

4. Conclusions

[13] The nighttime EIA and noontime EEJ display the same longitudinal structure on a ~1000 km horizontal scale during magnetically quiet periods around equinox. This leads to two main conclusions. The first is that the same large-scale modulation of the electric fields is modulating both systems. The second conclusion is that the longitudinal variation of the aforementioned large-scale electric field is controlled by a variation of the E-region dynamo. The variation in the E-region dynamo is produced by a longitudinal variation in the neutral winds associated with nonmigrating diurnal tides. We therefore conclude that the global-scale wavenumber-four longitudinal structure of the post-sunset EIA is determined by the E-region dynamo fields and associated upward drifts occurring in the dayside ionosphere. Other drivers of the EIA, such as the F-region dynamo with its strong vertical drifts around sunset or the nighttime vertical drifts associated with the E-region dynamo are not likely to be the cause of the observed longitudinal structure. The intriguing connection established here between space-based FUV and magnetic field observations may hold great potential for further studies of the equatorial ionosphere.

[14] **Acknowledgments.** The CHAMP mission is operated and supported by GeoForschungsZentrum Potsdam, the German Aerospace Center (DLR) and the German Federal Ministry of Education and Research (BMBF). The Ørsted and SAC-C projects received extensive support from the Danish government, the Argentine Commission on Space Initiatives, NASA, ESA, CNES and DARA. The IMAGE FUV instrument is supported by NASA at the University of California Berkeley. IMAGE FUV analysis is supported by NASA through Southwest Research Institute subcontract 8382 at the University of California Berkeley under contract NAS5-96020. The TIMED GUVI analysis was supported under NASA grant NAG5-5001 through the Aerospace Corporation under grant JO-7415. GSWM results are achieved on the CEDAR Data System at the National Center for Atmospheric Research sponsored by the National Science Foundation.

References

Doumouya, V., and Y. Cohen (2004), Improving and testing the empirical equatorial electrojet model with CHAMP satellite data, *Ann. Geophys.*, *22*, 3323–3333.

England, S. L., T. J. Immel, E. Sagawa, S. B. Henderson, M. E. Hagan, S. B. Mende, H. U. Frey, C. M. Swenson, and L. J. Paxton (2006), The effect of atmospheric tides on the morphology of the quiet-time post-sunset equatorial ionospheric anomaly, *J. Geophys. Res.*, 111, A10S19, doi:10.1029/2006JA011795.

Farley, D. T., E. Bonelli, B. G. Fejer, and M. F. Larsen (1986), The prereversal enhancement of the zonal electric field in the equatorial ionosphere, *J. Geophys. Res.*, *91*, 13,723–13,728.

Hagan, M. E., and J. M. Forbes (2002), Migrating and nonmigrating diurnal tides in the middle and upper atmosphere excited by tropospheric latent heat release, *J. Geophys. Res.*, *107*(D24), 4754, doi:10.1029/2001JD001236.

Heelis, R. A. (2004), Electrodynamics in the low and middle latitude ionosphere: A tutorial, *J. Atmos. Sol. Terr. Physics*, *66*, 825–838.

Henderson, S. B., C. M. Swenson, A. B. Christensen, and L. J. Paxton (2005a), Morphology of the equatorial anomaly and equatorial plasma bubbles using image subspace analysis of Global Ultraviolet Imager data, *J. Geophys. Res.*, *110*, A11306, doi:10.1029/2005JA011080.

Henderson, S. B., C. M. Swenson, J. H. Gunther, A. B. Christensen, and L. J. Paxton (2005b), Method for characterization of the equatorial anomaly using image subspace analysis of Global Ultraviolet Imager data, *J. Geophys. Res.*, *110*, A08308, doi:10.1029/2004JA010830.

Immel, T. J., E. Sagawa, S. L. England, S. B. Henderson, M. E. Hagan, S. B. Mende, H. U. Frey, C. M. Swenson, and L. J. Paxton (2006), The control of equatorial ionospheric morphology by atmospheric tides, *Geophys. Res. Lett.*, *33*, L15108, doi:10.1029/2006GL026161.

Ivers, D., R. Stening, J. Turner, and D. Winch (2003), Equatorial electrojet from Ørsted scalar magnetic field observations, *J. Geophys. Res.*, *108*(A2), 1061, doi:10.1029/2002JA009310.

Jadhav, G., M. Rajaram, and R. Rajaram (2002), A detailed study of equatorial electrojet phenomenon using Ørsted satellite observations, *J. Geophys. Res.*, *107*(A8), 1175, doi:10.1029/2001JA000183.

Kim, H. R., and S. D. King (1999), A study of local time and longitudinal variability of the amplitude of the equatorial electrojet observed in POGO satellite data, *Earth Planets Space*, *51*, 373–381.

Lühr, H., S. Maus, and M. Rother (2004), Noon-time equatorial electrojet: Its spatial features as determined by the CHAMP satellite, *J. Geophys. Res.*, *109*, A01306, doi:10.1029/2002JA009656.

Manoj, C., H. Lühr, S. Maus, and N. Nagarajan (2006), Evidence for short spatial correlation lengths of the noon-time equatorial electrojet: Inferred from a comparison of satellite and ground magnetic data, *J. Geophys. Res.*, doi:10.1029/2006JA011855, in press.

Maus, S., M. Rother, C. Stolle, W. Mai, S. Choi, H. Lühr, D. Cooke, and C.Roth (2006), Third generation of the Potsdam Magnetic Model of the Earth (POMME), *Geochem. Geophys. Geosyst.*, *7*, Q07008, doi:10.1029/2006GC001269.

Onwumechili, C. A., and C. E. Agu (1981), Longitudinal variation of equatorial electrojet parameters derived from POGO satellite observations, *Planet. Space Sci.*, *29*, 627–634.

Ravat, D., and W. J. Hinze (1993), Considerations of variations in ionospheric field effects in mapping equatorial lithospheric Magsat magnetic anomalies, *Geophys. J. Int.*, *113*, 387–398.

Rishbeth, H. (1971), Polarization fields produced by winds in the equatorial F-region, *Planet. Space Sci.*, *19*, 357–369.

Sagawa, E., T. J. Immel, H. U. Frey, and S. B. Mende (2005), Longitudinal structure of the equatorial anomaly in the nighttime ionosphere observed by IMAGE/FUV, *J. Geophys. Res.*, *110*, A11302, doi:10.1029/2004JA010848.

Tarpley, J. D. (1970), The ionospheric wind dynamo-II solar tides, *Planet. Space Sci.*, *18*, 1091–1103.

Thuillier, G., R. H. Wiens, G. G. Shepherd, and R. G. Roble (2002), Photochemistry and dynamics in the thermospheric intertropical arcs measured by the WIND Imaging Interferometer on board UARS: A comparison with TIE GCM simulations, *J. Atmos. Sol. Terr. Phys.*, *64*, 405–415.

S. L. England, T. J. Immel, and S. B. Mende, Space Sciences Laboratory, University of California, 7 Gauss Way, Berkeley, CA 94720-7450, USA. (england@ssl.berkeley.edu)

S. Maus, CIRES, University of Colorado, NOAA E/GC1, 325 Broadway, Boulder, CO 80305-3328, USA.